SUPPLEMENTAL MATERIALS: Supplemental Figures and Materials and Methods

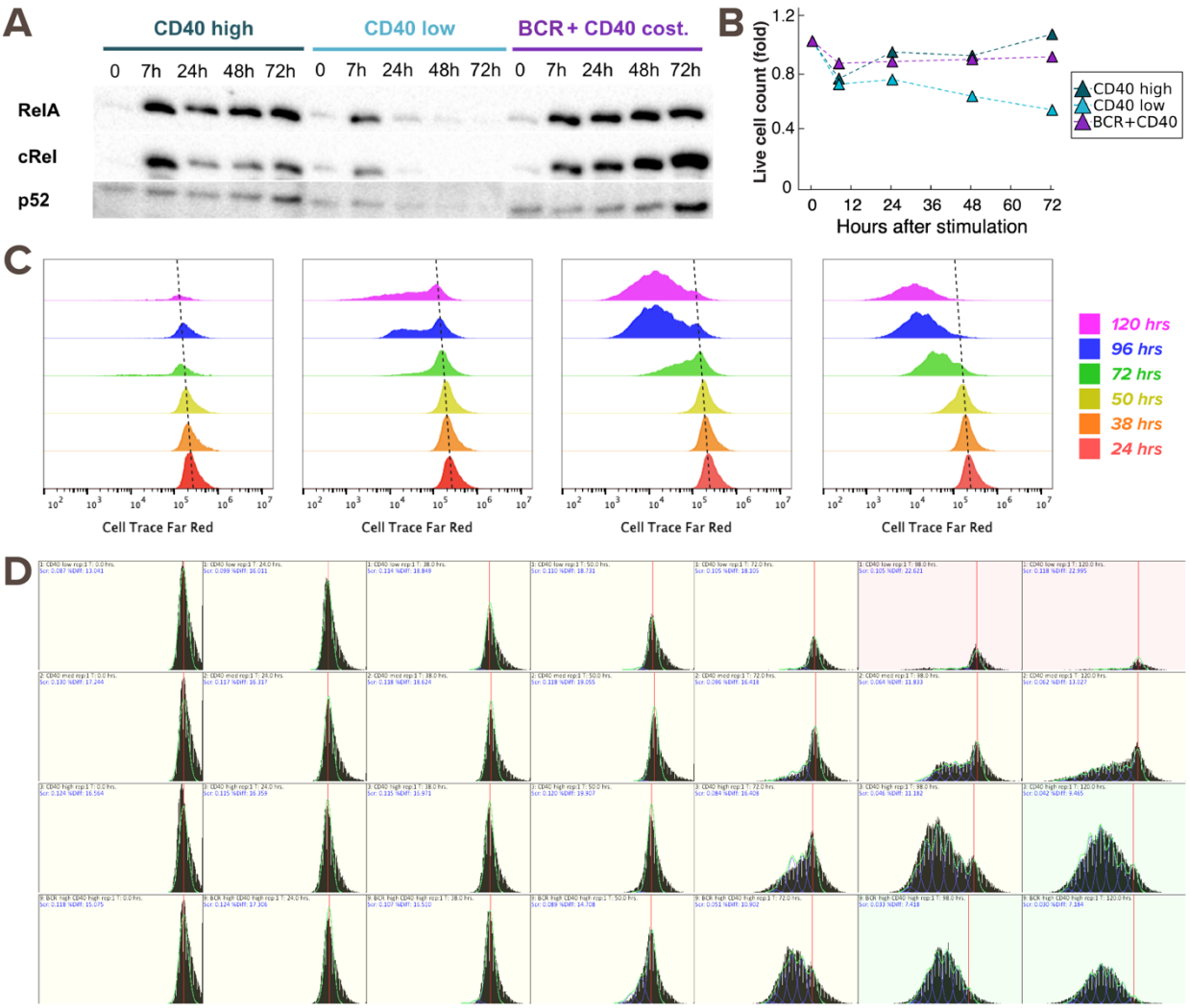

Figure S1. Raw experimental data to test the multi-scale B-cell model. (A) Immunoblot from experiments with 600K founder B-cells show nuclear RelA, cRel, and p52 levels at 0, 7, 24, 48, and 72hrs after stimulation with low α-CD40 (1μg/mL), high α-CD40 (10μg/mL), or costimulation with high α-CD40 and α-IgM (10μg/mL) . **(B)** Line graph of live B-cell count (fold-change) for each timepoint in (A), to which the samples are adjusted when loading to the gel. The cell count fluctuation is due to cell death, cell division, and technical error when transferring cells. **(C)** Cell Trace Far Red (CTFR) dye dilution fluorescence histogram for B-cells stimulated with (from left to right) low (1μg/mL), medium (3.3μg/mL), and high (10μg/mL) dose of α-CD40 and costimulation of high α-CD40 and α-IgM (10μg/mL). There is a baseline shift in CTFR fluorescence by about 2-fold from 24hrs to 120hrs (dotted line), which we adjusted when deconvolving the cells into each generation. **(D)** Deconvolution of the time courses in (C) into each generation, where the red line indicates the center of the undivided population of cells, the blue lines indicate individual proliferation peaks, and the green line represents the model sum.

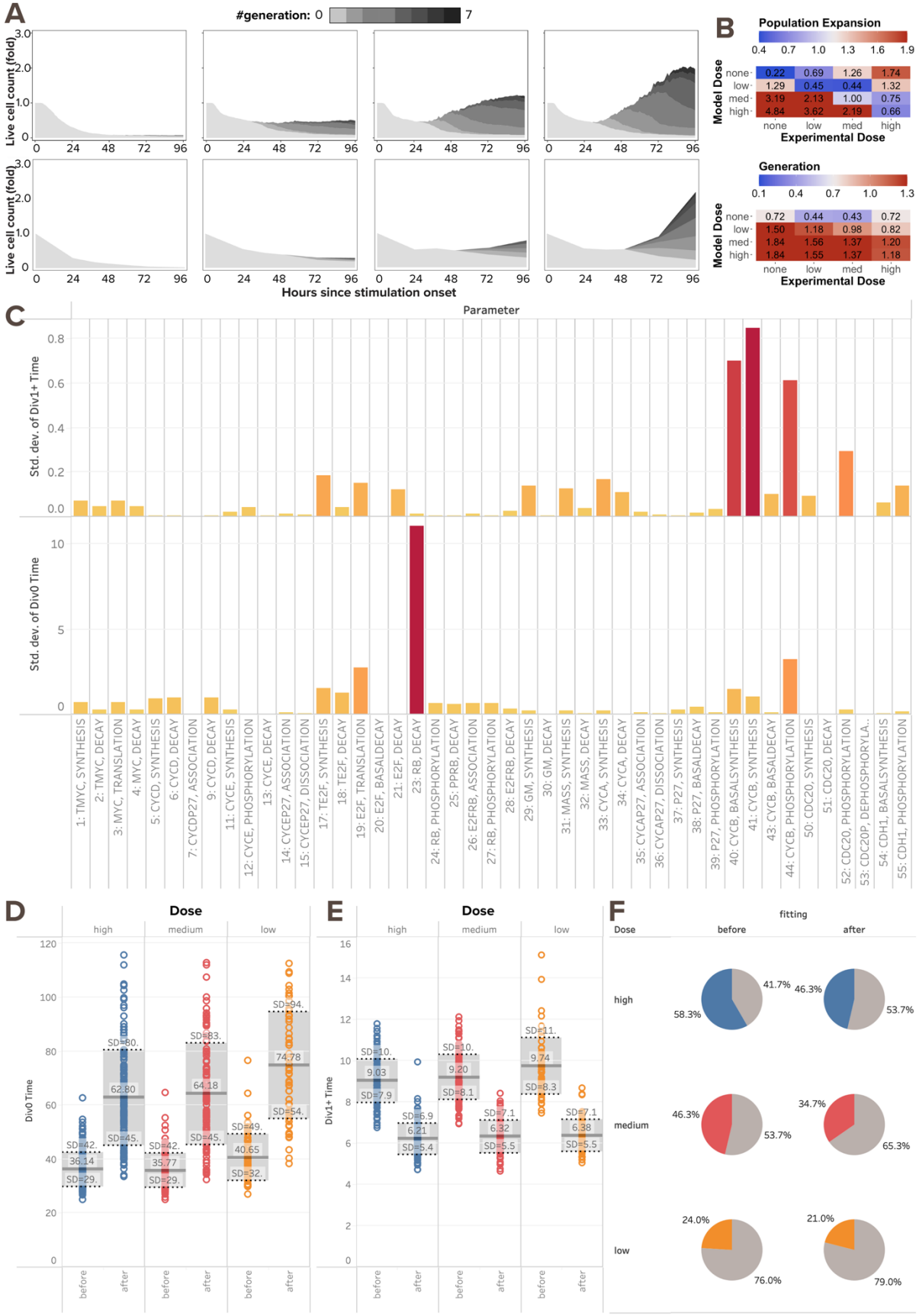

913

Figure S2. Multi-scale model needs tuning to recapitulate B-cell population dynamics in response to CD40 stimulation.
(A) Stacked area plots from model simulations of 1000 virtual B-cells (top) and matching experiments with 19196 founder B-cells (bottom) show their population dynamics in response to stimulation with (from left to right) no (0nM and 0μg/mL), low (6nM and 1μg/mL), medium (12nM and 3.3μg/mL), and high (30nM and 10μg/mL) dose of α-CD40. Each subsequent generation of proliferating cells is indicated with a darker gray. **(B)** Heatmap shows RMSD of relative population size expansion (top) and generation composition (bottom) in matching (diagonal) or mismatching (off-diagonal) model-and-experiment pairs. Some model doses (medium and low) are more deviated from their matching than mismatching experimental doses (high and medium, respectively), indicating a subpar fit. **(C)** Bar graph from local sensitivity analysis of parameters in the cell cycle module shows their standard deviations in time to first division (Tdiv0) and time to later divisions (Tdiv1+). Local sensitivity analysis is achieved by repetitive simulations that independently scaling each parameter in the cell cycle module by 0.2, 0.33, 0.4, 0.5, 0.66, 1.0, 1.5, 2.0, 2.5, 3.0, or 5.0-fold. 2 out of 55 parameters stand out as the best candidates for tuning Tdiv0 and Tdiv1+: retinoblastoma (Rb) decay rate and cyclin B (CycB) synthesis rate, respectively. These parameters were tuned in order to achieve a later and more dose-responsive Tdiv0, shorter Tdiv1+, and smaller divider percentage. **(D)** Box plots from model simulations of 300 virtual B-cells show the mean Tdiv0 increases for all doses after parameter tuning. **(E)** Box plots from model simulations of 300 virtual B-cells show the mean Tdiv1+ decreases for all doses after parameter tuning. **(F)** Pie charts from model simulations of 300 virtual B-cells show the percentage of dividing cells (colored slices) out of all founder cells decreases for all doses, while maintaining CD40 dose-responsiveness. Grey slices are the non-dividing founder cells that either die or survive without division.

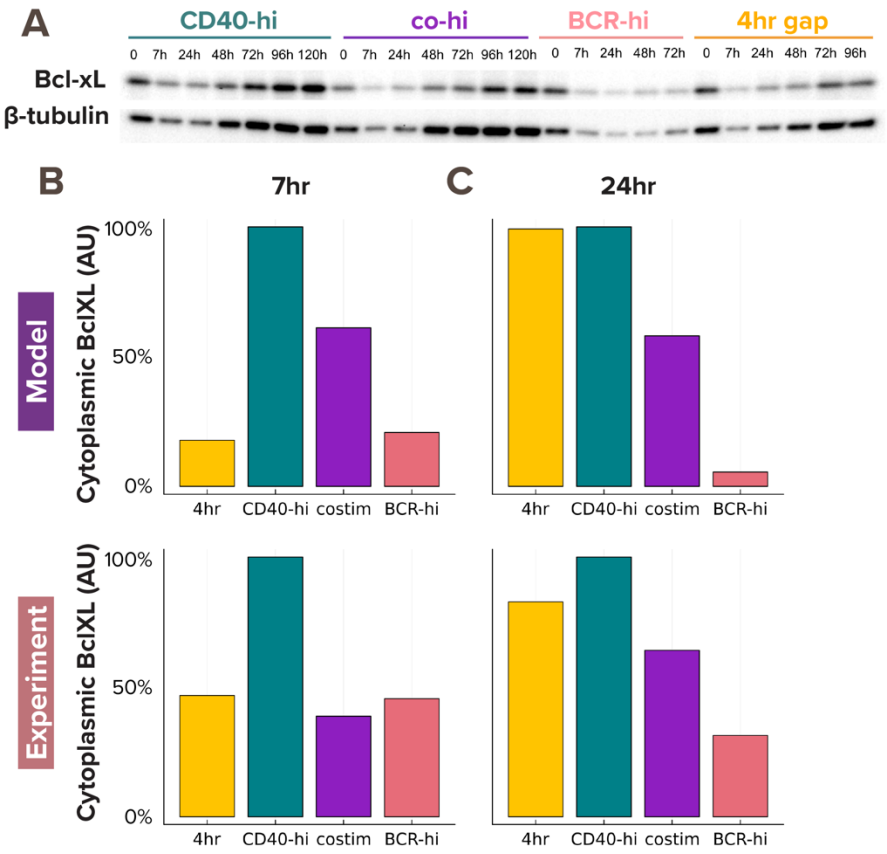

Figure S3. Model-simulated cytoplasmic BclXL level recapitulates experimental results. **(A)** Immunoblot from experiments with 600K founder B-cells show cytoplasmic Bcl-xL and β-tubulin levels in response to stimulation with (from left to right) high (10μg/mL) dose of α-CD40, high α-CD40 and high α-BCR, high α-BCR, and sequential stimulation of high α-BCR and high α-BCR with a 4hr delay. **(B-C)** Bar graphs from model simulations (top) and experiments (bottom) show consistent max-normalized quantification of cytoplasmic Bcl-xL level at **(B)** 7hrs and **(C)** 24hrs.

MATERIALS AND METHODS

Key Resources Table

REAGENT or RESOURCE	SOURCE	IDENTIFIER
Antibodies		
Rabbit polyclonal anti-RelA	Santa Cruz Biotechnologies	sc-372; RRID: AB_632037
Rabbit polyclonal anti-cRel	Santa Cruz Biotechnologies	sc-71; RRID: AB_2253705
Rabbit polyclonal anti-p50	Santa Cruz Biotechnologies	sc-114; RRID: AB_632034
Mouse monoclonal anti-Bcl-xL	Santa Cruz Biotechnologies	sc-8392; RRID: AB_626739
Rabbit polyclonal anti-p84	Abcam	ab131268
Mouse monoclonal anti-β-tubulin	Sigma Aldrich	T5201; RRID: AB_609915
HRP Anti-mouse secondary	Cell Signaling Technology	7076; RRID: AB_330924
HRP Anti-rabbit secondary	Cell Signaling Technology	7074; RRID: AB_2099233
CD40 monoclonal antibody (IC10)	Invitrogen	16-0401-86; RRID: AB_468940
Goat anti-mouse IgM	Jackson ImmunoResearch	115-066-020; RRID: AB_2338579
Chemicals, Peptides, and Recombinant Proteins		
Recombinant murine IL-4	PeproTech	214-14
Critical Commercial Assays		
CellTrace™ Far Red Proliferation Kit	ThermoFisher Scientific	C34564
SuperSignal West	ThermoFisher Scientific	34095, 34580
Experimental Models: Organisms/Strains		
Mouse: C57BL/6	The Jackson Laboratory	JAX: 000664; RRID: IMSR_JAX:000664
Software and Algorithms		
FlowJo V10.8.1	FlowJo LLC	N/A
FlowMax	Shokhirev et al., 2015 (Shokhirev and Hoffmann, 2013)	N/A
Python v3.7.164-bit base:conda	Anaconda v3.0	N/A

REAGENT or RESOURCE	SOURCE	IDENTIFIER
ImageJ2 v2.9.0		N/A
Julia v1.9.3		N/A
R v4.2.0		N/A

Mice

Mice were maintained in environmental control facilities at the University of California, Los Angeles. Female C57BL/6 mice in each replicate experiment were littermates, and were 8-13 weeks old unless otherwise indicated. Animal work was performed according to University of California, Los Angeles under approved protocols.

B cell isolation and culture

Spleens were harvested from 8–13-week-old female C57BL/6 mice. Homogenized splenocytes were incubated with anti-CD43 magnetic beads for 15 min at 4-8°C, washed with MACS buffer and passed through an LS column (Miltenyi Biotech). The purity of B cells was assessed at >97% based on B220 staining as described previously (Mitchell et al., 2018). Following isolation, B cells were stimulated with anti-CD40 (H: 10ug/mL, M: 3.3ug/mL, L: 1ug/mL), IL-4 (H: 20ng/mL, M: 6.6ng/mL, L: 2ng/mL), and anti-IgM (H: 10ug/mL, L: 1ug/mL), unless otherwise specified, and cultured for 4 days in fresh RPMI-based media at 37°C and 5% CO2. All anti-CD40 stimulation conditions mentioned in the results are stimulated with both anti-CD40 and IL-4 at corresponding doses.

Immunoblot

Cells were harvested from culture plates, washed in 1mL PBS and counted on a CytoFlex flow cytometer (CytoFLEX, Beckman Coulter), prior to preparing lysates for protein content analysis. Due to varying cell sizes and numbers over time as a result of growth and proliferation, an equal number of cells (as opposed to equal protein amounts) per sample was analyzed in each immunoblot. In cases where nuclear fractions were required to be separated, cells were first lysed in CE buffer on ice, followed by vortexing and centrifugation, and the supernatant containing the cytoplasmic fraction was removed. Nuclei were then lysed by 3 repeated freeze-thaw cycles between 37C water and dry ice, followed by centrifugation to clear the lysate of nuclear debris, after which the supernatant containing the nuclear fraction was harvested.

For immunoblotting, lysates were run on 4%–15% Criterion TGX pre-cast polyacrylamide gels (Bio-Rad), and transferred on to PVDF membranes using wet transfer. The following antibodies were used to identify the proteins of interest: RelA, cRel, Bcl-xL, p84 (loading control for nuclear lysates), and b-tubulin (loading control for cytoplasmic and whole cell lysates). Antibody details are given in the Resources table, and concentrations used were 1:5,000 for RelA and cRel, 1:1,000 for Bcl-xL, 1:10,000 for p84, and 1:10,000 for b-tubulin. Protein bands were detected using the Bio-Rad ChemiDoc XRS System, with a 10:1 mixture of the SuperSignal West Pico and Femto Maximum Sensitivity Substrates (Thermo Scientific) applied to detect chemiluminescence released by HRP-labeled secondary antibodies.

RelA, cRel, and Bcl-xL bands were quantified by measuring mean gray value using ImageJ2, deducting background value per lane (measured by a box of the same size directly below the target protein band), and normalizing intensities to the 0hr baseline.

Media and buffer compositions

B cell media: RPMI 1650 (Gibco) supplemented with 100 IU Penicillin, 100 µg/ml Streptomycin, 5 mM L-glutamine, 20 mM HEPES buffer, 1mM MEM non-essential amino acids, 1 mM Sodium pyruvate, 10% FBS, and 55 µM 2-Mercaptoethanol.
MACS buffer: Phosphate buffered saline, (pH 7.4) and 2% bovine serum albumin.
CE Buffer: 50 mM HEPES-KOH pH 7.6, 140 mM NaCl, 1 mM EDTA, 0.5% NP-40, freshly supplemented with EDTA-free protease inhibitors (5mM DTT, 1mM PMSF).
NE Buffer: 10 mM Tris-HCl, pH 8.0, 200 mM NaCl, 1 mM EDTA, freshly supplemented with EDTA-free protease inhibitors (5mM DTT, 1mM PMSF).

Measurement of generation-specific B cells by CTFR staining

B cells were stained with Cell Trace Far Red (CTFR) using CellTrace Far Red Cell Proliferation Kit (ThermoFisher Scientific, # C34564) as described by the manufacturer protocol. Briefly, 2M cells were resuspended in 1mL RT PBS and incubated with 1µL CTFR for 25 min at RT with rotation. Cells were washed by centrifugation, resuspension in 1mL RPMI with 10% FBS, and incubation for 10 min at RT. The washing steps were repeated 2 more times. CTFR labeled cells were treated with anti-CD40, IL-4, and / or anti-IgM for 96hrs as described above. The cells were harvested at indicated time points and acquired on the CytoFlex flow cytometer (CytoFLEX, Beckman Coulter). The cells were gated based on forward scatter (FSC) and side scatter (SSC) to identify live single cells. Doublets were then excluded from the analysis using FSC area and height. To deconvolve the cells into different generations based on dilution of CTFR, we used the Proliferation Modeling feature on FlowJo V10.8.1. Specifically, generation-0 cells were gated as "Undivided" in the APC-A channel according to the unstimulated control and 24hr samples, and the number of peaks were set based on visual estimation and then further adjusted based on the Peak Ratio and Root Mean Squared outputs to optimize curve fitting.

Computational modeling of the T-dependent receptor signaling pathway

The mathematical model of T-dependent (TD) B cell stimulation was developed in two parts. First, we expanded the previously published BCR-signaling ODE model (Shinohara *et al.*, 2014; Inoue *et al.*, 2016) by including the BCR receptor antigen binding (Fig. 1A left side), and scaled the parameters to match the units (nM^{-1} hr^{-1}) in the rest of our model. The Shinohara and Inoue models prescribed a signal function for the CBM complex, a downstream adaptor for BCR receptor. We bridged the gap between antigen concentration and CBM signaling with a few additional ODE equations, and tuned these additional parameters (Table 1) such that the signaling dynamics matched the previous version:

$$\frac{d}{dt}[ANTIGEN] = -\varphi_1 * [ANTIGEN] - \varphi_4[ANTIGEN] * [BCR] * C_{c2m} + \varphi_5 * [ABCR] * C_{c2m}$$

$$\frac{d}{dt}[BCR] = \varphi_2 - \varphi_3 * [BCR] - \varphi_4 * [ANTIGEN] * [BCR] + \varphi_5 * [ABCR]$$

$$\frac{d}{dt}[ABCR] = \varphi_4[ANTIGEN] * [BCR] - \varphi_5 * [ABCR] - \varphi_6 * [ABCR]$$

where $[ANTIGEN]$, $[BCR]$, and $[ABCR]$ are the concentrations of the antigen, BCR, and their complex; φ_i, $i = 1,2,3, \ldots$, are the reaction constants (index are listed in Table 1); $C_{c2m} = 0.01$ is a scaling factor for external ligands like ANTIGEN to convert cellular concentration to media concentration. In this model, $[ANTIGEN]$ is the model input corresponds to experimental stimulation α-BCR. As output of the BCR receptor module, $[ABCR]$ regulates CBM complex activation (Fig. 1A left side).

Next, we abstracted the CD40 model from its known signaling pathway (Elgueta *et al.*, 2009; Akiyama, Shinzawa and Akiyama, 2012) in a parsimonious way. As mentioned in the discussion, to avoid the complexity of combinatorial biochemical reactions among the TRAF complexes, we used TRAF3 to represent the TRAF2-TRAF3 complex that constitutively inhibits

the noncanonical NFκB pathway, and TRAF6 to represent the TRAF1-TRAF2, TRAF3-TRAF5, and TRAF6-TRAF2 complexes that all activate the canonical NFκB pathway.

$$\frac{d}{dt}[CD40L] = -\varphi_{11} * [CD40L] - \varphi_{14}[CD40L] * [CD40R] * C_{c2m} + \varphi_{15} * [CD40LR] * C_{c2m}$$

$$\frac{d}{dt}[CD40R] = \varphi_{12} - \varphi_{13} * [CD40R] - \varphi_{14} * [CD40L] * [CD40R] + \varphi_{15} * [CD40LR]$$

$$\frac{d}{dt}[CD40LR] = \varphi_{14}[CD40L] * [CD40R] - \varphi_{15} * [CD40LR] - \varphi_{16} * [CD40LR]$$

$$\frac{d}{dt}\left[TRAF6_{off}\right] = -\varphi_{17} * [CD40LR] * \left[TRAF6_{off}\right] + \varphi_{18} * [TRAF6_{on}]$$

$$\frac{d}{dt}[TRAF6_{on}] = \varphi_{17} * [CD40LR] * \left[TRAF6_{off}\right] - \varphi_{18} * [TRAF6_{on}]$$

$$\frac{d}{dt}[TRAF3] = \varphi_{19} * [TRAF3] - \varphi_{20} * [TRAF3] - \varphi_{21} * [CD40LR] * [TRAF3]$$

The subsequent kinases that further relay the receptor signal to NFκB signaling are TAK1 (for TRAF6) and NIK (for TRAF3). We used a Hill function for TRAF3-induced degradation of NIK to abstract a more complicated complex formation process:

$$\frac{d}{dt}[NIK] = \varphi_{35} - \varphi_{36} * [NIK] - \varphi_{37} * [NIK] * \frac{[TRAF3]^2}{[TRAF3]^2 + 0.5^2}$$

To generate heterogeneous cell responses, the receptor parameter values were distributed in each virtual B-cell the same way as the NFkB signaling module in previous publication, where synthesis, degradation, association, dissociation rates were drawn from a normal distribution with mean values from the standard parameter set (Table 1) and CV of 11.2% (Mitchell *et al.*, 2018). These ODEs (with 37 parameters and 12 species) were solved using the Tsit5 solver algorithm from the DiffEq.jl package in Julia, with an absolute error tolerance of 1e-5 and relative error tolerance of 1e-3. All simulations were carried out on an Ubuntu server with 64 threads, 2.1 to 3.7 GHz speed, and 384 GB RAM.

Multiscale modeling coupling signaling network and B cell proliferation

The receptor-extended TD model constructed above was combined with a published MATLAB model of B cell proliferation to create a multiscale model capable of simulating the division and death of a population of individual B-cells upon TD stimulation. The B cell model integrates a biophysically accurate model of canonical NFκB signaling (with about 300 parameters and 61 species) with models of the cell cycle (with 52 parameters and 23 species) and apoptosis (with 117 parameters and 59 species) (Shokhirev *et al.*, 2015; Mitchell *et al.*, 2018) to create a multiscale model capable of simulating the division and death of a population of individual cells upon T-dependent stimulation. Cleaved PARP (cParp) in the apoptosis model and cadherin-1 (Cdh1) concentration thresholds in the cell cycle model triggered virtual B-cell death and division, respectively. We translated the model from MATLAB into Julia 1.9.3 for faster execution. All reactions and parameters within the NFκB, apoptosis and cell cycle networks were maintained and distributed as described by Mitchell et al. (Mitchell *et al.*, 2018), except for 2 parameters in the cell cycle network that were changed to reduce the discrepancy between CD40 and CpG-induced proliferative response (Fig. S2, see more details in “Local sensitivity analysis to tune CD40-activated cell fates” section of the Methods).

Separate modules of the multi-scale model were employed when simulating for different purposes. For the NFκB dynamics in figure 1, only the receptor-NFκB model was used for the simulation, and the cell fate modules (apoptosis and cell cycle) were excluded. For Fig. S2C-F when we tuned the CD40-activated cell fates, the cell death module was excluded to enable faster turnaround for parameter tuning in the cell cycle module. For Fig. 5B-D, the cell cycle

module was excluded to isolate the effects of BCR signaling on cell survival. All the other model simulation used the full multi-scale model. When we reported the population trajectory of NFκB activity in Fig. 1E-H, all 1000 cells contributed to the mean and standard deviation, but in Fig. 4G-J, only cells that are alive at each timepoint contributed to the mean and standard deviation.

All of the code to run the model simulations and plot the figures is provided on GitHub (https://github.com/helengracehuang/BCR-CD40-integration). For each virtual B-cell with its own set of parameters, we ran the model in two phases to first identify the steady state, and then simulate the dynamic time course upon stimulation, with initial states from this steady state. The steady state was solved using Julia's steady state Tsit5 solver with an absolute error tolerance of 1e-5 and relative error tolerance of 1e-3. The simulation time for which the given ODE reach steady state was limited within 800hrs.

Computational modeling of the BCR-induced cell death pathway

Since we found α-BCR stimulation had an NFκB-independent anti-survival effect that overrides its NFκB-dependent pro-survival effect (Fig. 3), we decided to resolve this difference by modifying the multi-scale model. It was reported that ligation of the BCR induces cell death in some B cells (Graves, Craxton and Clark, 2004) due to activation of Bcl-2 Interacting Mediator of cell death (Bim) (Gao, Kazama and Yonehara, 2012), caspase-2 or -8 (Chen *et al.*, 1999), mitochondrial dysfunction (Akkaya *et al.*, 2018) or more. Based on these signaling mechanisms that may mediate activation-induced cell death (AICD) in B-cells and the available species in the existing cell death module, we revised the cell death module of the T-dependent multi-scale B-cell model to include a simplified pathway from activated BCR to caspase-8 processing (Fig. 4A):

$$\frac{d}{dt}[PC8] = \left(original\ \frac{d}{dt}[PC8]\right) - \varphi_{C8,AICD} * [PC8] * [ABCR]$$

$$\frac{d}{dt}[C8] = \left(original\ \frac{d}{dt}[C8]\right) + \varphi_{C8,AICD} * [PC8] * [ABCR]$$

where $[PC8]$, $[C8]$, and $[ABCR]$ are the concentrations of the pre-caspase-8, caspase-8, and activated BCR; $original\ \frac{d}{dt}[PC8]$ and $original\ \frac{d}{dt}[C8]$ are the original differential equations for pre-caspase-8 and caspase-8 in Mitchell *et al.*, 2018, abbreviated to highlight the revision we made; $\varphi_{C8,AICD}$ was tuned to be 0.00021 according to experimental data of BCR-CD40 costimulation versus CD40-only stimulation conditions (Fig. 4B-C).

Simulations prior to figure 4 and Fig. 5F-H did not include this BCR-induced cell death pathway. Fig. 4B-F, Fig. 5A-E, I-K, and figures 6 and 7 were all simulated with the modified caspase-8 equations.

Model fit evaluation

Root-mean-squared deviation (RMSD) were calculated on the population dynamics between model simulation and experimental results (Fig. 2F, S2B, 3E, 3F, and 4D) and between two experimental conditions (Fig. 3H,K) in the same manner. Two RMSD scores, one for population expansion index (Fig. 2D), and the other for generational composition (Fig. 2E) between each pair of model and experimental outputs at each experimental timepoint (0, 24, 36, 48, 72, and 96hrs) were calculated.

For the RMSD on generational composition:

$$RMSD_{gen} = \sqrt{\sum_{i=1}^{5}\sum_{j=0}^{6}\left(\frac{n_{i,j}}{N_i} - \frac{\hat{n}_{i,j}}{\hat{N}_i}\right)^2}$$

Where i is the i-th timepoint of the experimental measurement (i.e. $i = 1$ corresponds to the measurement at 24 hours, followed by 36, 48, 72, and 96 hours), and j is the generation number, ranging from generation 0 to 6 corresponding to founder cells to cells that have divided 6 times. $n_{i,j}$ thus means the number of live cells in generation j and timepoint i in the experimental data, while $\hat{n}_{i,j}$ is the corresponding live cell number in generation j and timepoint i in model simulation. Additionally, $N_i = \sum_{j=0}^{6} n_{i,j}$ represents the total number of live cells at timepoint i in the experimental data, and $\hat{N}_i = \sum_{j=0}^{6} \hat{n}_{i,j}$ represents the corresponding total live cell number in model simulation. $\frac{n_{i,j}}{N_i}$ and $\frac{\hat{n}_{i,j}}{\hat{N}_i}$ are thus the generation decomposition ratios at each time point for experimental data and simulation data, respectively.

For population expansion, the RMSD is composed of two parts, one normalized to population size at 0 hour (N_0) and one normalized to the population size at 24 hours (N_1) to account for unpredictable mechanical cell death (which typically occur within the first few hours) as a form of technical error in experiments. Both RMSD scores are then normalized to the number of timepoints (5 timepoints for 0hr normalization, and 4 timepoints for 24hr normalization) and the maximum population expansion so that different amount of population expansion at different doses are evaluated on the same scale:

$$RMSD_{pop\_exp} = \sqrt{\frac{\sum_{i=1}^{5}\left(\frac{N_t}{N_0} - \frac{\hat{N}_t}{\hat{N}_0}\right)^2}{5 \cdot \max\limits_{i=1,\ldots,5} N_i}} + \sqrt{\frac{\sum_{i=2}^{5}\left(\frac{N_t}{N_1} - \frac{\hat{N}_t}{\hat{N}_1}\right)^2}{4 \cdot \max\limits_{i=2,\ldots,5} N_i}}$$

Local sensitivity analysis to tune CD40-activated cell fates

Due to the discrepancy between CD40 and CpG-induced proliferative response, we quantified several key variables in the dye dilution data that determined the population dynamics with FlowMax (Shokhirev and Hoffmann, 2013). After fitting FlowMax model to the experimental data, we quantified the time to first division (Tdiv0), time to later divisions (Tdiv1+), and the fraction of generation 0 cells that respond by dividing (F0) in response to low, medium, and high CD40 doses. In all CD40 doses, the average Tdiv0 is much later and more dose-specific (68.5 to 76.9hrs since stimulation onset for high to low dose of CD40) than what the model predicted (36.1 to 40.6hrs). On the other hand, the average Tdiv1+ of the CD40 experimental data were mostly shorter than predicted by the model (Table S1 Exp vs Model(1), Fig. S2A), and the proportion of dividers was lower, indicated by a larger amount of cells in generation 0 at 96hrs in Fig. S2A and a smaller F0 quantified by FlowMax than the model predicted (Table S2 Exp vs Model(1).

To improve model fit, we identified locally sensitive parameters in the cell cycle module that contribute to Tdiv0 and Tdiv1+ by calculating the standard deviation in division times when scaling each parameter by 0.2, 0.33, 0.4, 0.5, 0.66, 1.0, 1.5, 2.0, 2.5, 3.0, or 5.0-fold. 2 out of 55 parameters stood out as the best candidates for tuning Tdiv0 and Tdiv1+: retinoblastoma (Rb) decay rate and cyclin B (CycB) synthesis rate, respectively (Fig. S2C). Rb decay rate was tuned to be 10% of the original value, whereas CycB was tuned to be 1.8-fold the original value to achieve a later and more dose-responsive Tdiv0, shorter Tdiv1+, and smaller divider percentage (Fig. S2D,E,F).

A simulation of 300 cells with distributed parameters before and after parameter tuning showed that mean Tdiv0 for dividers increased from 36.14 hours to 62.80 hours for high dose of CD40 stimulation, and from 40.65 hours to 74.78 hours for low dose, achieving both a later and more dose-responsive Tdiv0, resulting in much more agreement with the FlowMax output based on experimental data (Table S1, left 3 columns). The mean Tdiv1+ for dividers decreases from around 9 hours to 6 hours for all doses, which is in concordant with high dose of CD40, but in less agreement with medium and low doses (Table S1, right 3 columns). Table S2 also showed the percentage of dividers out of all founder cells decreased for all doses, while maintaining CD40 dose-responsiveness.

Table S1. Experimental vs. Model proliferation time before (1) & after (2) tuning

Condition	EXP Tdiv0	MODEL(1) Tdiv0	MODEL(2) Tdiv0	EXP Tdiv1+	MODEL(1) Tdiv1+	MODEL(2) Tdiv1+
CD40 high	68.5	36.1	60.7	6.1	9.0	6.2
CD40 medium	68.6	35.7	66.2	7.8	9.2	6.0
CD40 low	76.9	40.6	79.4	35.2	9.7	6.3

Table S2. Experimental vs. Model divider percentage before (1) & after (2) tuning

Condition	EXP F0	MODEL(1) F0	MODEL(2) F0
CD40 high	46.8%	58.3%	46.3%
CD40 medium	18.4%	46.3%	34.7%
CD40 low	4.4%	24.0%	21.0%